



Research article

The application of ferrous and graphitic N modified graphene-based composite cathode material in the bio-electro-Fenton system driven by sediment microbial fuel cells to degrade methyl orange

Minmin Sun^a, Chengxian Wang^{b,*}^a Shanghai Renhong Engineering Consulting Co., Ltd, 1599 Huibin Road, Qingpu District, Shanghai, 201700, China^b State Key Laboratory of Pollution Control and Resource Reuse, College of Environmental Science and Engineering, Tongji University, 1239 Siping Road, Shanghai, 200092, China

ARTICLE INFO

Keywords:

Bioelectrochemical system
Methyl orange
Graphene-based composite cathode materials
Bio-electro-Fenton system
Advance oxidation process

ABSTRACT

In this work, the ferrous (Fe^{2+}) and graphitic N modified graphene-based composite cathode materials (N-rGO/ Fe_3O_4) were developed through an in-situ reduction method, aiming to facilitate the two-electron pathway in the oxidation-reduction process. This approach generated a specific concentration of H_2O_2 , enabling the construction of a sediment bio-electro-Fenton system using Fe^{2+} released from the cathode materials. Notably, this system operates without the need for proton exchange membranes. During the cathode material preparation, the utilization of Fe^{2+} as a reduction agent for graphene oxide (GO), triggered ammonia water to form graphitic N in graphene sheets. This addition enhanced the two-electron pathway, resulting in increased H_2O_2 production. Specifically, when the Fe^{2+} concentration was maintained at 0.1 mol/L, precise preparation of N-rGO/ Fe_3O_4 occurred, leading to a maximum output voltage of 0.528 V and a maximum power density of 178.17 mW/m^2 . The degradation of methyl orange (MO) reached 68.91% within a 25-h period, a phenomenon contributed to the presence of graphitic N in the graphene sheets. H_2O_2 , a byproduct of the two-electron pathway in cathode oxidation reduction reaction, played a crucial role in constructing the bio-electro-Fenton system. This system, in conjunction with Fe^{2+} released from N-rGO/ Fe_3O_4 , facilitated the complete degradation process of MO.

1. Introduction

The bioelectrochemical system (BES), a technology demonstrating significant practical potential, comprises anode and cathode reaction regions, and/or a separation membrane, functioning in microbial fuel cell (MFC) and microbial electrolysis cell (MEC) modes. These modes convert the biomass energy stored in the organic matter into electricity [1,2], with MFC generating electricity during organic matter degradation. Various MFC structures, such as dual-chamber MFC [3], plant MFC [4], air cathode MFC [5], sediment MFC (SMFC) [6], has been researched. In cathodes utilizing O_2 as an electron acceptor two distinct oxygen reduction reaction (ORR) mechanisms exist [7]: a four-electron pathway involving a direct reaction among O_2 , electrons and protons, and a two-electron

* Corresponding author.

E-mail address: Wang3359@tongji.edu.cn (C. Wang).<https://doi.org/10.1016/j.heliyon.2024.e24772>

Received 30 September 2023; Received in revised form 22 November 2023; Accepted 14 January 2024

Available online 20 January 2024

2405-8440/© 2024 Published by Elsevier Ltd.

This is an open access article under the CC BY-NC-ND license

<http://creativecommons.org/licenses/by-nc-nd/4.0/>.

pathway leading to hydrogen peroxide production with a high overpotential [2,8]. Significantly, the utilization of a separation proton exchange membrane (PEM) is deemed unnecessary for SMFC due to its potential to shorten the lifespan of the reactor.

While previous studies indicated that electricity generation in SMFC can be enhanced by increasing multiple anodes, which can strengthen the anode surface area, and reducing the distance between anodes and optimizing their spatial arrangement, sediment characteristics also significantly influence SMFC performance and microbial community structure [9]. The choice of anode and cathode materials plays a crucial role in SMFC performance, leading to extensive researches on new materials, such as Fe(III) oxide [10, 11], graphene-based materials [12] and carbon nanotube [13,14], etc. The different cathodic materials can drive either two or four electron transfer pathways. In addition, the accumulation of electrons in the cathode reaction region via the external circuit provides an opportunity to construct the electro-Fenton (E-Fenton) process when the H_2O_2 is present in the cathode region with Fe^{2+} as catalyst [15]. This SMFC-driven E-Fenton process, termed bio electro-Fenton system (Bio-E-Fenton), offers continuous degradation of bio-refractory organics, including antibiotics [16], polychlorobiphenyls [17], azo dye [18], etc.

However, azo dyes pose a common environmental pollutant challenge in dye manufacturing and the paint industry, with pollution severity increasing due to rapid economic development. Advance oxidation process (AOP), including photochemical oxidation [19], catalytic wet oxidation [20], sonochemical oxidation [21], ozone oxidation [22], Fenton oxidation [23] and electrochemical advanced oxidation [24,25], are considered efficient technologies for azo dye treatment. Nevertheless, the high cost limits the practice application of AOPs in industrial manufacture. The Bio-E-Fenton system, derived from AOPs, enables the degradation of refractory organics in the dual microbial fuel cell [15]. Bio-electro-Fenton (BEF) systems have been studied as a promising technology to achieve environmental organic pollutants degradation and bioelectricity generation [26]. A novel bio-electro-Fenton system was developed with dual application for the catalytic degradation of tetracycline antibiotic in wastewater and bioelectricity generation. The system was able to achieve up to $99.04 \pm 0.91\%$ tetracycline degradation after 24 h under optimal conditions [27]. Despite the advantages of this technology, there are still problems to consider including low production of current density, chemical requirement for pH adjustment, iron sludge formation due to the addition of iron catalysts and costly materials used [26,28].

In this work, we synthesized the 3D magnetic graphene material, characterized by its graphitic nitrogen content, to effectively enhance the two-electron pathway. This study aims to the decolor and degradation of methyl orange (MO), a representative azo dye, within the SMFC system. Furthermore, the bacterial species of anode and cathode colonies was also investigated, contributing to the understanding of microbial dynamics in this unique bioelectrochemical system. This work not only contributes to the advancement of bioelectrochemical systems, but also introduces a promising avenue for addressing environmental challenges associated with azo dye pollution.

2. Materials and methods

2.1. Chemicals and materials

Carbon felt (CF) was purchased from Sichuan Junrui carbon fiber material Co. Ltd. Polymeric sponge (PS) was purchased from Dongguan Junfeng rubber & plastic sponge Co., Ltd. All chemicals, meeting analytical grade standards, were obtained from Shanghai Aladdin biochemical technology Co., Ltd. Throughout the experiment, de-ionized water was employed.

2.2. Pretreatment of anode electrode

The CF, serving as anode electrode, underwent pretreatment and was subsequently cut into $4.5 \text{ cm} \times 4.5 \text{ cm}$ pieces. The CF pieces underwent ultrasonication in propyl alcohol, ethyl alcohol and deionized water for 30 min each. Subsequently, they were dried under a vacuum at $60 \text{ }^\circ\text{C}$ overnight.

2.3. Cathode electrode fabrication

Graphite oxide was synthesized using a modified Hummer's method as the previous articles [3]. Specifically, graphite oxide powder was dispersed and ultrasonicated in 100 mL of deionized water for 12 h. Then, the dispersion was centrifuged for 20 min at 4000 r.p.m. to remove the unexfoliated graphite oxide particles. And then, the suspension solution of graphene oxide (GO) should be obtained.

PS, as the skeleton of the cathode materials, was cut into $5.0 \text{ cm} \times 5.0 \text{ cm}$ pieces, which was immersed into 1 mg/L GO dispersion solution for 30 min, and dried in the air. This process should be repeated three times to enhance the load of GO in PS skeleton. And then, PS pieces were soaked into 0.5 M FeCl_2 solution and heated in water bath at $80 \text{ }^\circ\text{C}$ for 12 h to reduce GO to reduced graphene oxide (rGO). When the solution cooled down to room temperature, ammonium hydroxide was used to adjust the pH value of this solution to 11, which was sealed and heated in water bath at $90 \text{ }^\circ\text{C}$ for 6 h. After washing the PS skeleton multiple times, the graphite nitrogen modified magnetic graphene can be obtained, marked as rGO/ Fe_3O_4 . With the different pH value (pH = 5, 7 and 11), the products were $\alpha\text{-FeOOH}$, $\beta\text{-FeOOH}$ and Fe_3O_4 , marked as N-rGO/ $\alpha\text{-FeOOH}$, N-rGO/ $\beta\text{-FeOOH}$ and N-rGO/ Fe_3O_4 , respectively.

To examine the influence of the magnetic material (Fe_3O_4) ratio in the composite material on the removal efficiency of MO by SMFC, various FeCl_2 concentrations ($\text{Fe}^{2+} = 0, 0.01, 0.05, 0.1, \text{ and } 0.2 \text{ mol/L}$) were utilized to prepare N-rGO/ Fe_3O_4 . These are denoted as Fe0, Fe10, Fe50, Fe100, and Fe200, respectively.

2.4. Construction and operation of SMFC

SMFC was assembled with a cylindrical container ($\varphi 150 \text{ mm} \times 250 \text{ mm}$), consisted of two layers as schematically shown in Fig. 1. The top of SMFC was the cathode, in which the oxygen reduction reaction among the electrons, O_2 and organic matter was occurred on the surface of rGO/ Fe_3O_4 electrode. The lower section of the SMFC primarily consists of the graphite felt serving as the anodic electrode, securely buried in the organic sediment sludge sourced from the Dai River in Qinhuangdao, Hebei Province, China. This arrangement is designed to prevent the inhibitory effects of oxygen diffusion from the cathode chamber on the electricity-producing microorganisms. The thickness of the sediment was 15 cm, and 500 mL 10 mg/L MO solution was added into the container, which was based on a balance between ensuring a measurable impact on the system while maintaining a practical relevance to environmental scenarios. There is a graphite felt and a rGO/ Fe_3O_4 modified PS under/above the solid-liquid interface 10 cm and 5 cm, respectively. These anode and cathode electrodes should be connected by copper wire with a 1000Ω external resistance. The cathode part SMFC was continuously aerated at 100 mL/min to supply enough oxygen as the terminal electron acceptor. All SMFCs in this study were operated at $35 \pm 1 \text{ }^\circ\text{C}$ which had little effect on electricity generation.

2.5. Characterization methods

The detection of H_2O_2 was carried out using the dimethoxyphenol (DMP) spectrophotometric method [29]. The methyl orange (MO) solution was also analyzed using spectrophotometry [30]. The determination of total iron and ferrous iron concentrations was carried out using the *ortho*-phenanthroline spectrophotometric method [31].

The voltage of SMFC (U) was monitored every 1 min across a 1000Ω load (R_{ex}) by a 16-channel data acquisition system (LR6116A, Sino Measure Automation Tech, Co., Ltd., Hangzhou, China). Open circuit potential (OCP) was recorded during the stable electricity generation period. Current (I) can be calculated according to the Ohm's Law ($U=IR$), where R is the fixed external resistance in the circuit. The voluminal power density (W/m^3) and current density (A/m^2) were normalized by the working volume of the anode chamber according to the basic electrical relation. The polarization and power density curves were determined by changing the external resistance from $20 \text{ k}\Omega$ to 50Ω . Stable voltages were recorded at 30 min intervals to evaluate the electricity output of the MFCs.

The microstructure and morphology of N-rGO/ Fe_3O_4 modified PS were analyzed with scanning electron microscopy (SEM; Phenom pro). The Brunauere-Emmette-Teller (BET) surface area and porosity of the samples were evaluated based on nitrogen sorption isotherms, which were measured at 77 K using an automatic adsorption instrument (Micromeritics, 3H-2000PM2, Beijing). The surface elements of these materials were detected by X-ray photoelectron spectroscopy (XPS, Thermal Scientific ESCALB 250Xi spectrometer, USA), and the XPS data was fitted by the software of XPS Peak 4.1.

2.6. High-throughput sequencing

To investigate changes in the microbial community before, during stable operation, and after the operation of the bio-electro-Fenton system, samples were extracted at various stages, including the pre-operation phase, stable operational phase, and post-operation phase, specifically focusing on the microbial community changes in the anodic biofilm. Following extraction, the samples underwent centrifugation for 5 min at 4000 g, and the supernatant was discarded. The samples were then stored at $-20 \text{ }^\circ\text{C}$ prior to DNA extraction. DNA extraction was performed using the E.Z. N.A. Soil DNA Kit (OMEGA, D5625-01, USA) according to the

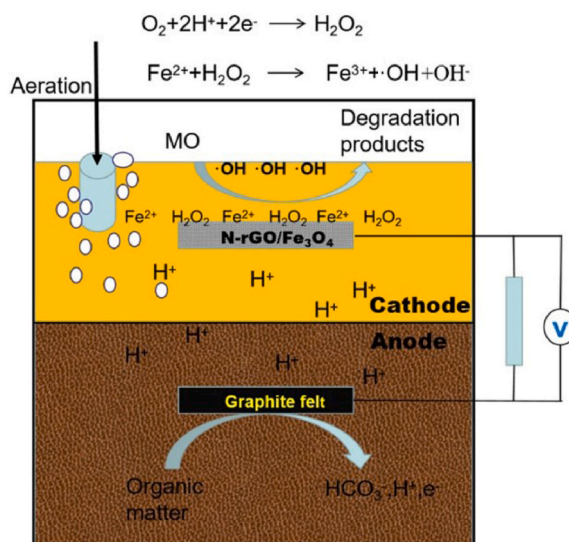


Fig. 1. Schematic illustration of sediment microbial fuel.

manufacturer's instructions. Subsequently, 30 ng of sludge was utilized, and the V3–V4 region of the bacterial 16S rRNA gene was amplified by PCR. After electrophoresis, target pure PCR products were obtained by cutting bands from 0.8% (w/v) agarose gels. DNA purification was carried out using the AxyPrep DNA Gel Extraction Kit (Axygen Biosciences, Union City, CA, U.S.), following the manufacturer's guidelines. DNA quantification was conducted using QuantiFluor™-ST (Promega, U.S.). The DNA fragments were then subjected to the preparation of adapters with tags, followed by ligation. The library was enriched through PCR amplification. Illumina MiSeq platform-based DNA sequencing of the library (10 nM) was performed in accordance with standard protocols and conducted by Shanghai Majorbio Bio-pharm Technology Co., Ltd (Shanghai, China).

3. Results and discussion

3.1. Microstructure characterization of the cathode material

The morphologies of N-rGO, N-rGO/ α -FeOOH, N-rGO/ β -FeOOH and N-rGO/Fe₃O₄ were examined using scanning electron microscopy (SEM). In Fig. 2(a), the crumpled and thin structures were typical of rGO, prepared by the modified Hummer's method. Due to the quantity variance of NH₃·H₂O with different pH value, nitrogen-modified rGO with three different iron compounds, like α -FeOOH, β -FeOOH and Fe₃O₄, were produced. At a pH value of 5, petal-like lamella α -FeOOH grew on the surface of N-rGO (Fig. 2(b)). As the pH value increased to 7, numerous N-rGO/ β -FeOOH particles appeared on the surface of rGO sheets (Fig. 2(c)). In contrast, Fe₃O₄ nanoparticles were formed and evenly distributed on the surface of N-rGO nanosheet when the pH value reached 11 (Fig. 2(d)), consistent with the specific surface area of N-rGO/Fe₃O₄. According to the International Union of Pure and Applied Chemistry (IUPAC) [32], the Brunauer-Emmerr-Teller (BET) specific surface area of these samples, determined based on the nitrogen isothermal adsorption curve (Fig. 3), is as follows: N-rGO (106.092 m²·g⁻¹), N-rGO/ α -FeOOH (83.412 m²·g⁻¹), N-rGO/ β -FeOOH (47.275 m²·g⁻¹), and N-rGO/Fe₃O₄ (133.680 m²·g⁻¹). The hysteresis loops (Type H3) indicate the plate-like particle aggregates (N-rGO/ α -FeOOH), leading to slit-shaped pores (N-rGO/ β -FeOOH and N-rGO/Fe₃O₄). The structural changes observed in these materials should be contributed to the variation in the quantity of NH₃·H₂O at different pH value, influencing the production process. To investigate the surface compositions of these materials, XPS spectrums were examined, as shown in Fig. 3(e–h). The analysis revealed that N-rGO/Fe₃O₄ contained C (56.23%), N (6.64%), O (32%) and Fe (5.12%). The high-resolution C 1s spectrum of N-rGO/Fe₃O₄ exhibited two major components corresponding to C–C (284.5 eV) and C=N (285.0 eV) [33]. Peaks at binding energies of 530.5 eV and 533.0 eV were assigned to O=C–NH₂ and O–C, respectively (Fig. 3(f)). Additionally, two sub-peaks at 398.7 eV (Fe–N_x) and 401.5 eV (graphitic N) were observed. The presence of Fe–N bonding (398.7 eV) in the high-resolution N 1s XPS spectrum demonstrated the formation of Fe–N_x group in N-rGO/Fe₃O₄ (Fig. 3(g)), suggests successful doping of nitrogen in the reduced graphene oxide (rGO) and the formation of Fe–N_x active sites, which are crucial for enhancing the electrocatalytic activity of the material. The Fe–N_x sites can significantly improve the material's performance in various applications, such as energy storage and conversion, catalysis, and

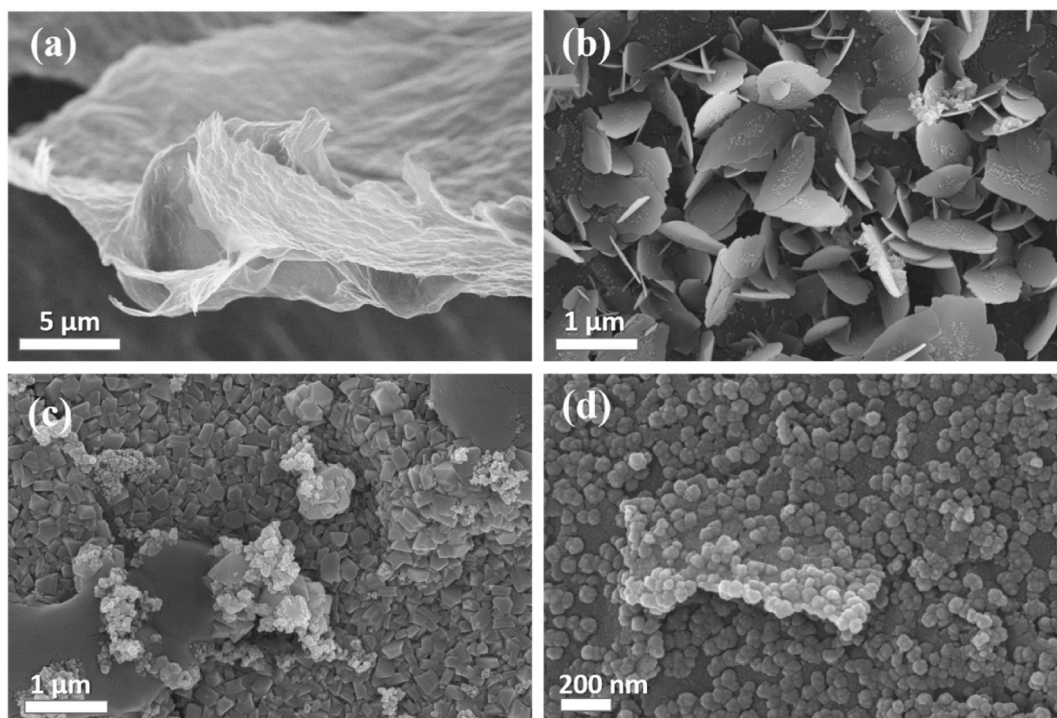


Fig. 2. SEM images of N-rGO (a), N-rGO/ α -FeOOH (b), N-rGO/ β -FeOOH (c) and N-rGO/Fe₃O₄ (d).

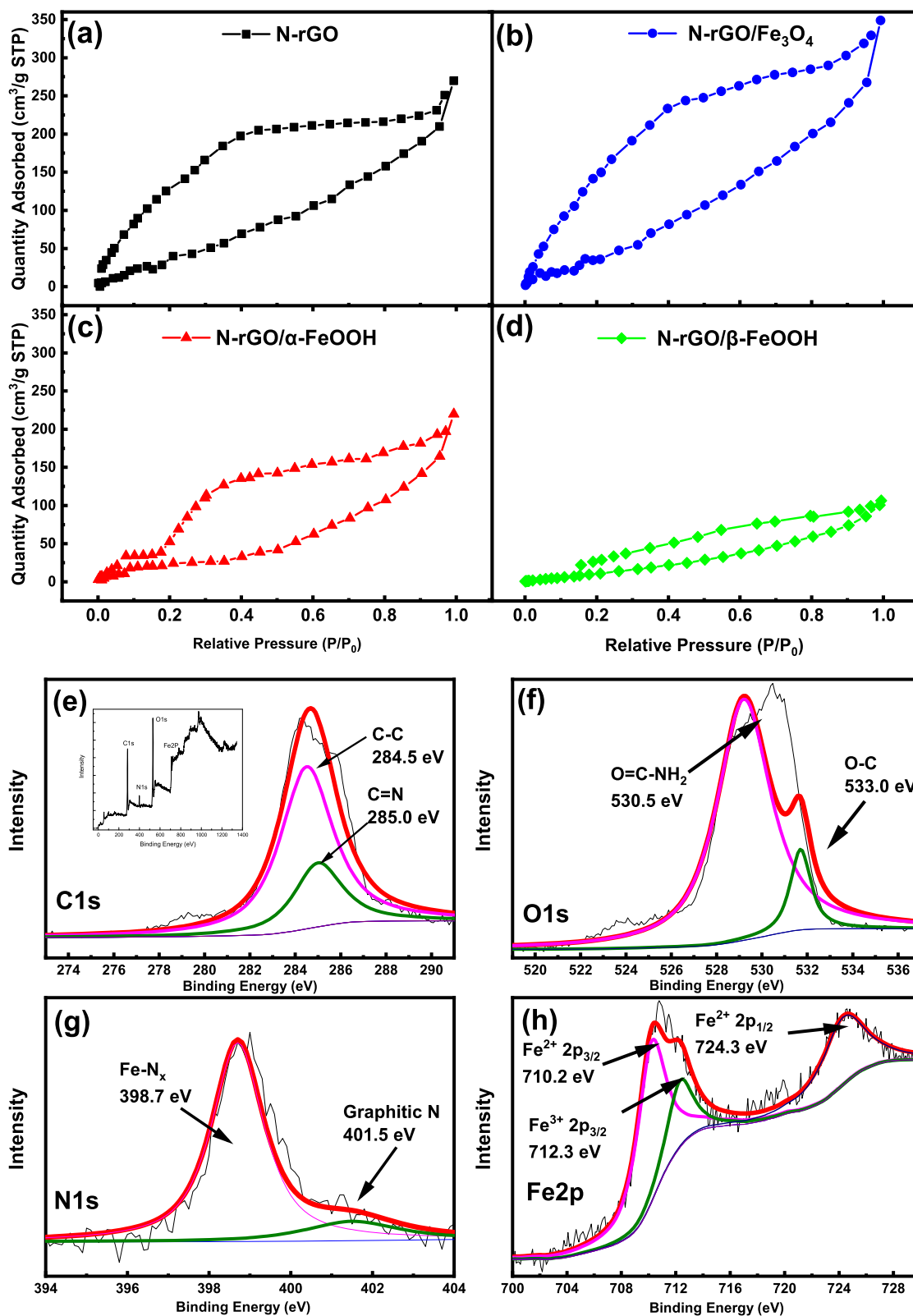


Fig. 3. Nitrogen isothermal adsorption curves of N-rGO (a), N-rGO/Fe₃O₄, (b) N-rGO/ α -FeOOH (c), and N-rGO/ β -FeOOH (d); High-resolution XPS spectrum of N-rGO/Fe₃O₄ (insert of e) with C1s (e), O1s (f), N1s (g) and Fe 2p (h).

environmental remediation [34,35]. Similarly, the binding energy peaks at 710.2 and 724.3 eV were corresponding to Fe 2p_{3/2} and Fe 2p_{1/2} [36], respectively. The absence of the charge transfer satellite peak at 717 eV indicated the formation in mixed oxides of Fe(II) and Fe(III) such as Fe₃O₄ [37,38]. In addition, XPS spectrums of N-rGO, N-rGO/ α -FeOOH and N-rGO/ β -FeOOH were also measured, and the nitrogen content of N-rGO, N-rGO/ α -FeOOH and N-rGO/ β -FeOOH were 3.13%, 5.28% and 6.08%, respectively (Fig. SI 1-3).

3.2. The electricity generation performance of bio-electron Fenton system

To explore the electricity generation performance of these SMFCs equipped with a kind of bio-electron Fenton system, marked as N-rGO/ α -FeOOH, N-rGO/ β -FeOOH and N-rGO/Fe₃O₄, these reactors were operated using inoculum from the bottom mud of Dai River, Qinhuangdao, Hebei province, China. These SMFCs reactors were initiated in an open circuit with a rapid start-up speed. Subsequently, 1000 Ω external resistances applied to the closed circuits of each reactor. As depicted in Fig. 4(a), the voltage of these reactors increased significantly after 10 days of operating and stabilized after 20 days. The stable voltage for N-rGO/ α -FeOOH, N-rGO/ β -FeOOH and N-rGO/Fe₃O₄ were 0.482, 0.500 and 0.528 V, respectively. The long-term electricity generation stability (LEGS) is a critical parameter for assessing the stability of electricity generation. It is defined as the duration required for the system to stabilize within a 20% amplitude range of the maximum voltage during a stable operational period [3]. The LEGS of N-rGO/Fe₃O₄ was 90 h, surpassing that of N-rGO/ α -FeOOH (20 h) and N-rGO/ β -FeOOH (40 h) by 4.5 times and 2.5 times, respectively. After 60 days of operation, the voltage of N-rGO/ α -FeOOH, N-rGO/ β -FeOOH suddenly dropped down, leading to a low maximum power density. As shown in Fig. 4 (b), the maximum power density was 178.17 mW/m², exceeding N-rGO/ α -FeOOH (60.3 mW/m²) and N-rGO/ β -FeOOH (98.2 mW/m²) by 2.9 times and 1.8 times, respectively. Moreover, the internal resistance of N-rGO/ α -FeOOH, N-rGO/ β -FeOOH and N-rGO/Fe₃O₄ was 1050, 1200 and 350 Ω , indicating that the higher catalytic activity than N-rGO/ α -FeOOH and N-rGO/ β -FeOOH. In addition, the steeper polarization slope in N-rGO/Fe₃O₄ compared to N-rGO/ α -FeOOH and N-rGO/ β -FeOOH suggested that a higher current density of N-rGO/Fe₃O₄ might imply a better reaction catalyst activity and electron transfer rate.

3.3. Degradation of MO with bio-electron Fenton system

As depicted in Fig. 5, the degradation of MO was evident, with similar curves observed for all three materials. In this experiment, the initial concentration of MO was 10 mg/L for each bio-electronic Fenton system. The concentration of the cathodic liquid was then monitored at 2-h intervals to illustrate the MO degradation, as shown in Fig. 5 (a). The concentrations of MO exhibited a steep decline in the first 5 h, followed by a steady decrease over the next 25 h. This suggested that the MO, as an azo dye, could be function as an electron acceptor, particularly when the MO concentration reached a certain level. Noticeable variations in the degradation performance of methyl orange (MO) among different materials in the Sediment Microbial Fuel Cell (SMFC) become apparent within the initial 75 h of operation. N-rGO/Fe₃O₄ achieved a degradation rate of 68.9%, slightly higher than N-rGO/ α -FeOOH (65.5%) and N-rGO/ β -FeOOH (61.5%). To verify that the degradation of MO should be contributed to the bio-electron Fenton reaction of cathode materials, rather than the adsorption function of anode sediment, the contrast experiments were conducted between the open and the closed circuit. Specifically, one set of the experiments were connected a 1000 Ω external resistance in the closed circuit, and the other was cut off the circuit. As shown in Fig. 5(b), the removal rate of N-rGO/ α -FeOOH, N-rGO/ β -FeOOH and N-rGO/Fe₃O₄ with the open circuit was all changed slightly within 80 h. However, it was significantly function to degrade the MO when the circuit was closed, indicating that the adsorption of anode sediment played a limited or negligible role in MO degradation.

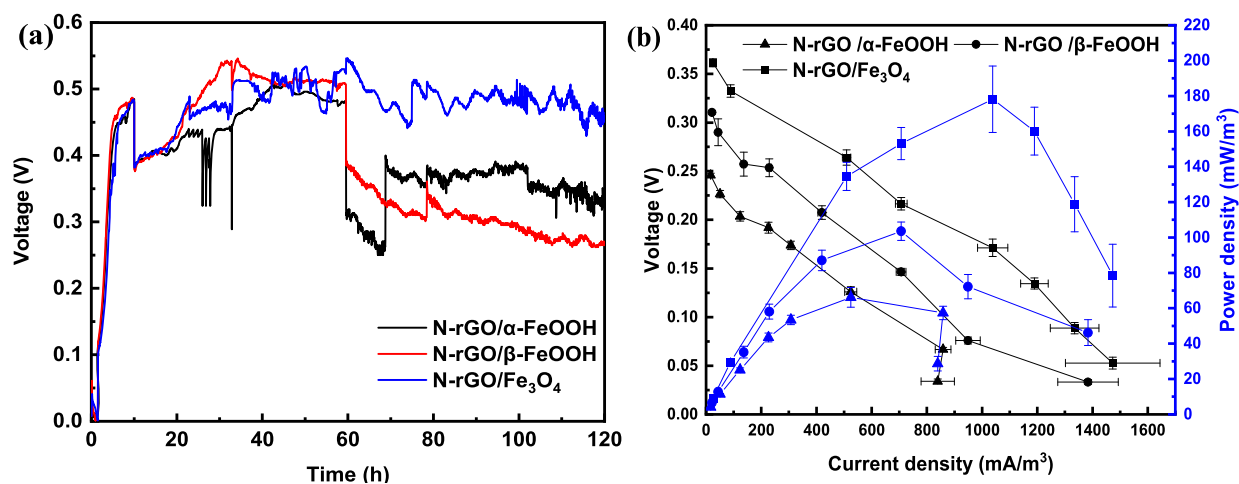


Fig. 4. System power generation performance of three cathode materials: system electricity generation diagram (a), and polarization curve and power density (b).

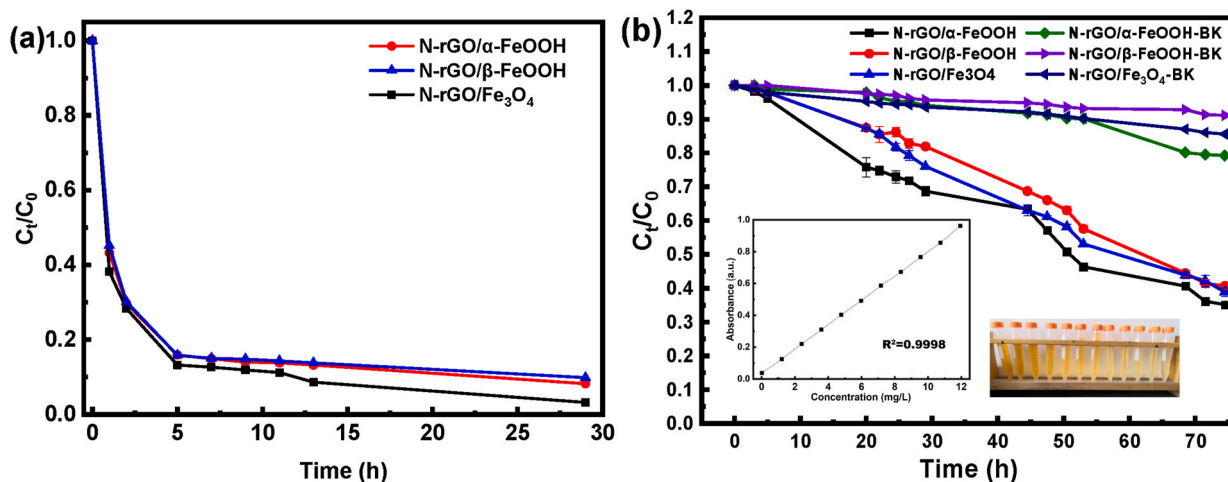


Fig. 5. Two degradation stages of MO by three bioelectric Fenton systems: the adsorption process of sediment (a), and the degradation process of bio-E-Fenton system (b).

3.4. The functional mechanism of magnetic graphene 3D materials

The bio-electron Fenton system, a facet of the microbial fuel cell technology, combined Fenton technology, electrochemical technology and biotechnology, offering a unique advantage in degrading refractory organic matter. The electricigens in the anode sediment, especially inside the anode material, can decompose organic matter, generating proton and equivalent electron. In detail, electrons flow through the external circuit, where they participate in the cathodic reaction with the proton moving through the solid-liquid interface between the anode sediment and cathode liquid. When oxygen serves as the acceptor, two kinds of oxidation reduction reaction (ORR) occurred. One is the four-electron pathway, in which the direct reaction can proceed among O_2 , electrons and protons as shown in Equation (a). And the other is the indirect reaction with the product, H_2O_2 , in the two-electron pathway as seen in Equation (b). So, the concentration of H_2O_2 and iron ions should be measured to indicate the reaction activity of the bio-electron Fenton system. The Fenton reaction processes were shown as Equation (b) and (c). However, there were many adverse reactions occurred in these processes, like Equation (d-h). The pH can also influence the selectivity between the two-electron ($2e^-$) and four-electron ($4e^-$) oxygen reduction reaction (ORR). ORR experiments include the pH dependences of $2e^-$ versus $4e^-$ ORR selectivity [39].

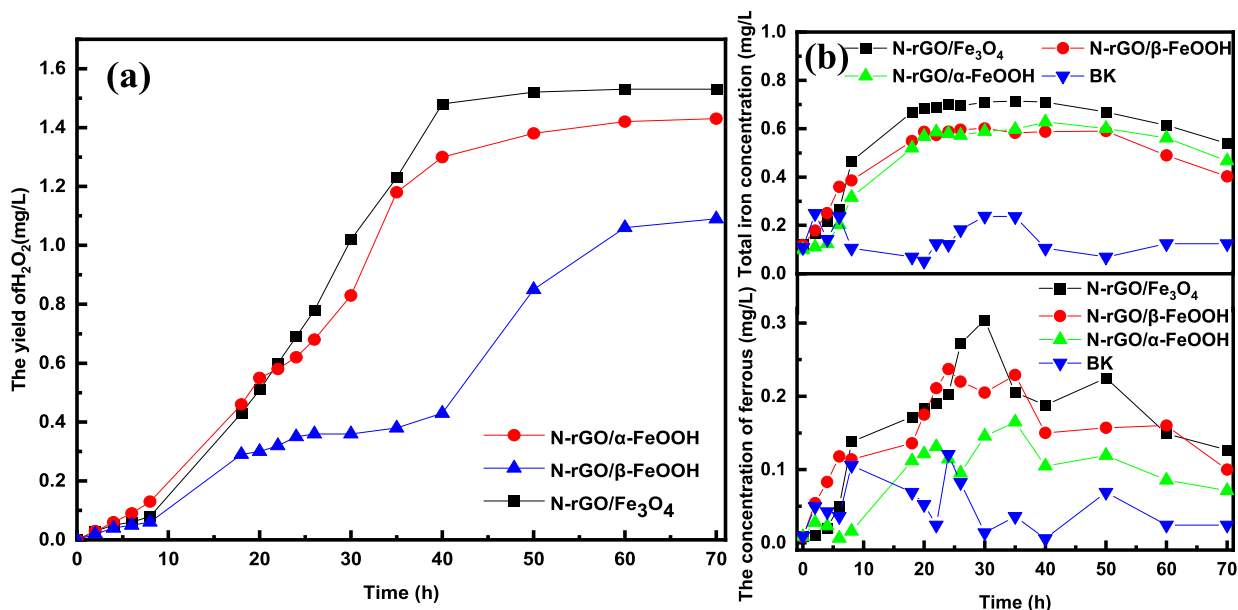


Fig. 6. H_2O_2 yield (a) and the released Fe curves (b) of various cathode materials.



To explore the catalytic activity of the cathode materials, the yield of H_2O_2 was measured for N-rGO/ α -FeOOH, N-rGO/ β -FeOOH and N-rGO/ Fe_3O_4 using the DMP method. As shown in Fig. 6(a), there was a consistent trend of H_2O_2 yield, with a rapid initial increase within the first 40 h. The maximum H_2O_2 yield of N-rGO/ α -FeOOH and N-rGO/ Fe_3O_4 was 1.42 mg/L and 1.53 mg/L, respectively, reached at the 45th hour, which was 10 h earlier than that of N-rGO/ β -FeOOH (1.09 mg/L). In addition, the concentration of ferrous ions increased throughout the operation. When the released Fe^{2+} attained a balance with the in situ produced Fe^{2+} , the concentration of ferrous would be fluctuated in small range. The total iron concentration was remained at a stabilized level, correlating with the initial concentration of Fe^{2+} during material preparation, as evident in Fig. 6(b). It was notable that both the concentration of Fe^{2+} and H_2O_2 yield for N-rGO/ Fe_3O_4 were both higher than that for N-rGO/ α -FeOOH and N-rGO/ β -FeOOH.

To investigate the effect of magnetic material (Fe_3O_4) ratio in composite material proportion on the removal performance of MO by SMFC, the electricity generation performance was assessed within the SMFC cathode range, varying Fe^{2+} concentration. Results shown

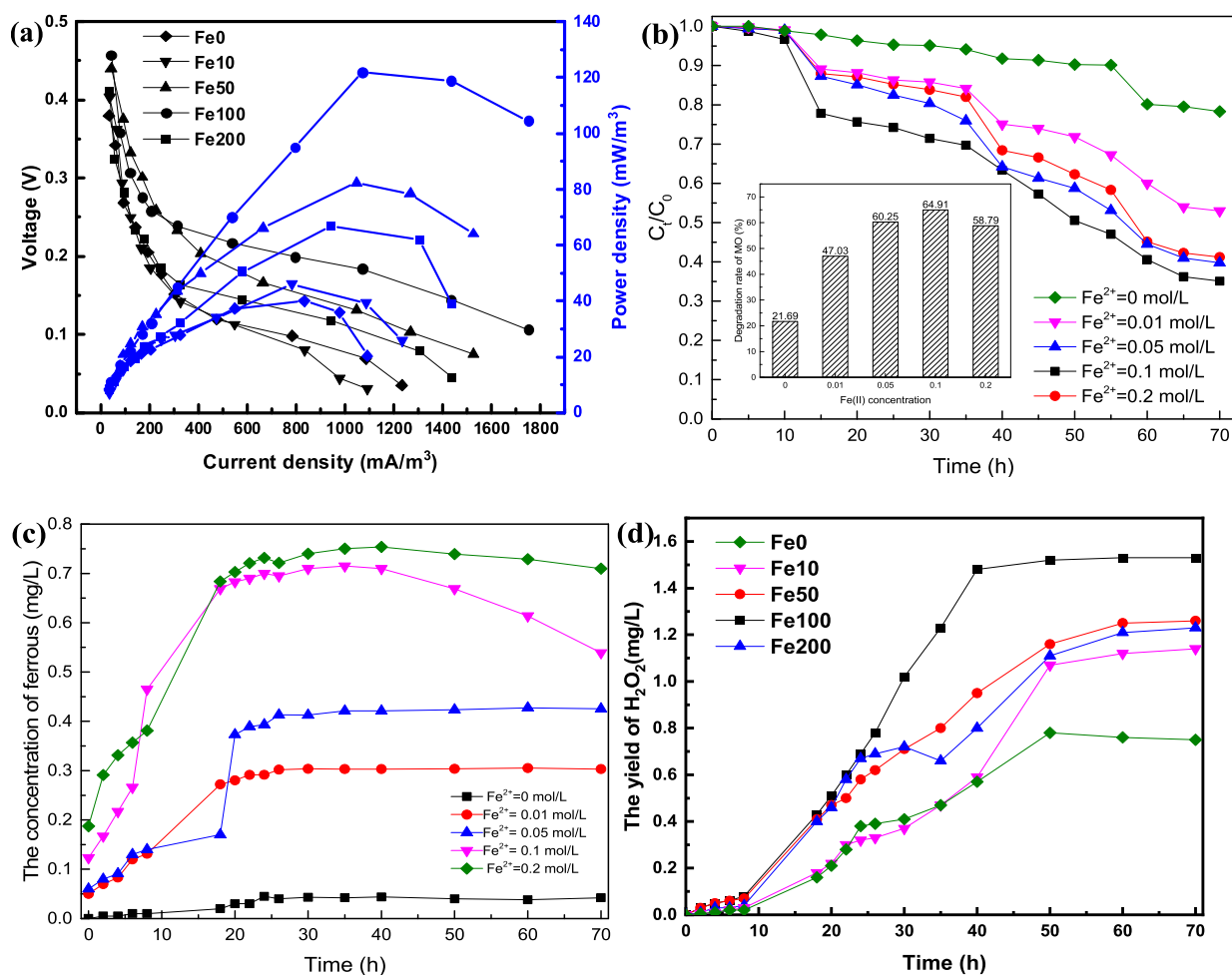


Fig. 7. Polarization curve and power density (b), the MO degradation rate (b), the released Fe (a) and H_2O_2 yield curves (b) of cathode materials with various Fe^{2+} in bioelectric Fenton systems.

that the maximum power density at different Fe^{2+} concentration ($\text{Fe}^{2+} = 0, 0.01, 0.05, 0.1$ and 0.2 mol/L) was 40.03, 46.09, 82.37, 121.88 and 66.83 mW/m^3 , respectively. This suggests that the inclusion of Fe^{2+} as a modified element in cathode material significantly influenced SMFC electricity generation, as shown in Fig. 7(a). When the concentration of Fe^{2+} was up to 0.1 mol/L, the open circuit voltage (OCV) was 0.48 V with a high electricity generation stability (Fig. SI 4). Meanwhile, the removal rate of MO in SMFC cathode materials with different Fe^{2+} concentration was explored, lasting for 70 h as shown in Fig. 7(b). With Fe^{2+} concentration increased, the degradation rate of MO firstly increases and then drops, suggesting that Fe^{2+} was of great significance to produce H_2O_2 and degrade the MO in cathode range, and the most suitable concentration of Fe^{2+} was 0.1 mol/L. Furthermore, the concentration of ferrous and H_2O_2 in catholyte was measured as shown in Fig. 7(c and d). It was observed that the ferrous ions could be detected in catholyte without the Fe^{2+} ($\text{Fe}^{2+} = 0$ mol/L) in the cathode material, which was ascribed to the diffusion effect from the sediment to the catholyte, and the hydrogen peroxide was produced in a low level, indirectly indicating these new materials could promote the hydrogen peroxide.

In addition, with Fe^{2+} concentration increased, more Fe^{2+} ions were released from the cathode materials to the catholyte. When the initial Fe^{2+} added into GO dispersion solution was 0.1 mol/L, the ferrous concentration in catholyte was similar to that of 0.2 mol/L, indicating that 0.1 mol/L Fe^{2+} ions could exactly reduce 1 mg/L GO to rGO. Consequently, the Fe^{2+} ions released from the cathode materials and H_2O_2 generated in catholyte together constituted Fenton system. Graphic nitrogen played an important role in the production of H_2O_2 . In order to produce Fe_3O_4 , which exhibited optimal performance in electricity generation and the degradation of MO in SMFC, the pH value of these cathode materials during preparation process were all adjusted to 11, except for the blank group ($\text{Fe}^{2+} = 0$ mol/L). In the absence of Fe^{2+} ions in the blank group, the electricity generation process leaned towards the four-electron pathway (Equation (a)), leading to a high voltage (the average voltage was 0.55 V in Fig. SI 4). With Fe^{2+} concentration increasing, the dosage of ammonia water was increased. When the concentration of Fe^{2+} was 0.1 mol/L, the dosage of FeCl_2 was equal to ammonia. From Fig. 7(d) we can know, the H_2O_2 production in the cathode materials increased at first and then reduced ($\text{Fe}^{2+} = 0.1$ mol/L) along with the increase of Fe^{2+} ions. The production of H_2O_2 in the cathode materials in a bio-electro-Fenton system driven by SMFC can be influenced by the concentration of Fe^{2+} ions. Initially, as the concentration of Fe^{2+} ions increase, the production of H_2O_2 also increases. This is because Fe^{2+} ions can react with H_2O_2 to produce hydroxyl radicals via the Fenton reaction [26]. This reaction is beneficial for the degradation of organic pollutants and can enhance the performance of the SMFC [26]. However, as the concentration of Fe^{2+} ions continue to increase, the production of H_2O_2 may decrease. This could be due to several reasons: (1) At high concentrations of Fe^{2+} , the

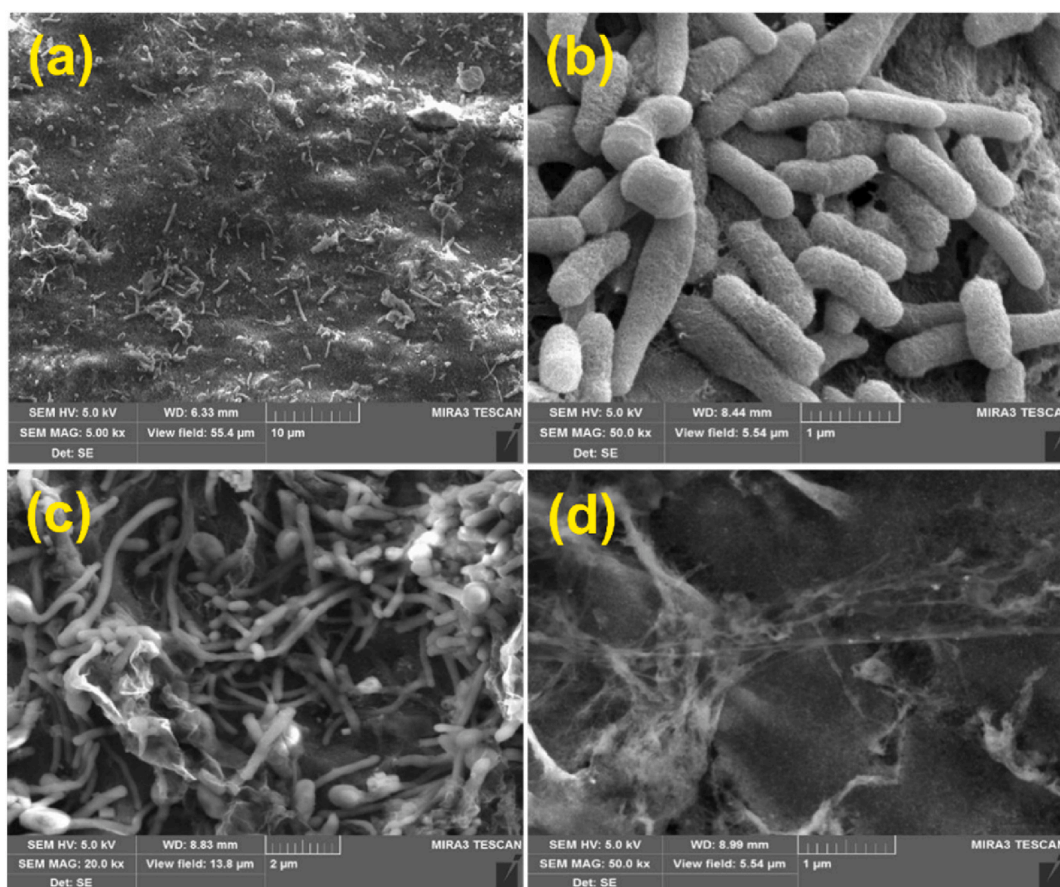


Fig. 8. SEM images of the anodic deposits in SMFC with N-rGO/ Fe_3O_4 as anode material: rod-shaped bacteria (a and b), filamentous bacteria (c) and nanowires (d).

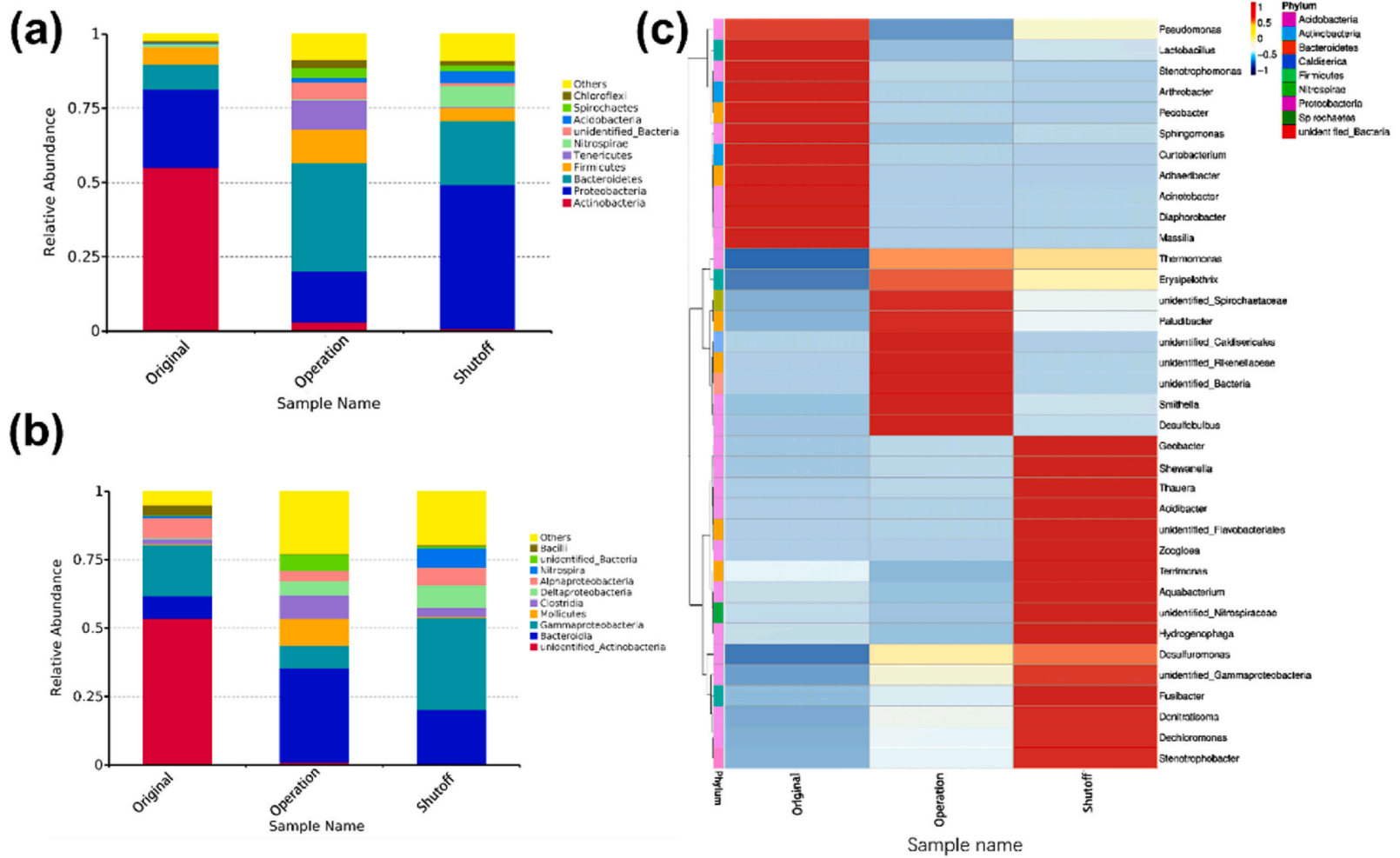


Fig. 9. Top 10 microbial community structures at the phylum level (a) and class level (b), and hierarchical clustering heatmap of the top 35 species at the genus level (c).

reaction may reach a saturation point, beyond which additional Fe^{2+} ions do not contribute to an increase in H_2O_2 production [40]; (2) High concentrations of Fe^{2+} ions can also lead to side reactions that consume H_2O_2 , reducing its overall production [26]. (3) Excess Fe^{2+} ions can lead to catalyst poisoning, where the active sites on the catalyst surface are blocked, reducing the efficiency of the reaction [41]. In addition, the pH plays a pivotal role in influencing H_2O_2 production, MO degradation, and the selectivity of electron pathways in a bio-electro-Fenton system driven by SMFC. Monitoring the pH behavior in the cathode is crucial for a comprehensive understanding of these processes. The pH of the solution significantly impacts H_2O_2 production and MO degradation in a bio-electro-Fenton system powered by a sediment microbial fuel cell (SMFC) [39]. Additionally, the pH of the solution is a key factor affecting the production of H_2O_2 , and the catalysts' performance is highly dependent on electrolyte pH values [42]. The formation rate of H_2O_2 remains constant between pH 2 and 7 but increases exponentially above pH = 8 [43]. Furthermore, the degradation of MO is favored with increased catalyst loading and reaction time.

3.5. Succession of microbial community structure

After achieving stable operation of the bio-electro-Fenton system, we conducted an observation and analysis of the morphology and ecology of microorganisms on the anode membrane surface using scanning electron microscopy (SEM). The SEM images in Fig. 8 illustrated the microbial colony morphology on the anode electrode surface, revealing that rod-shaped bacteria predominantly cover the electrode surface. This observation signified the development of a biofilm structure where microorganisms from the sludge made direct contact with the electrode (Fig. 8(a) and (b)). The biofilm, composed of numerous microbial colonies, indicated that a higher microbial content enhances the system's capability to decompose organic matter in the sediment, converting more chemical energy into electricity. This strengthened the overall bio-electro-Fenton reaction. Furthermore, Fig. 8(c) highlighted the formation of abundant nanowire-like structures, often referred to as "nano-wires" (Fig. 8(d)), between microorganisms. These nano-wires played a crucial role in facilitating electron transfer between microorganisms, effectively boosting the voltage of the bio-electro-Fenton system.

To explore the dynamic shifts in the anodic microbial community structure within the Bio-electro-Fenton system, a comparative analysis was conducted at the phylum, class, and genus levels for the original sludge (Original), anodic sludge during system operation (Operation), and anodic sludge after system shutdown (Shutoff). This investigation aimed to scrutinize and analyze microbial fluctuations and the succession of dominant bacterial groups during different operational stages of the Bio-electro-Fenton system. The Venn diagram visually represented the unique and shared microbial species among the samples. Fig. SI 5 illustrates the Venn diagram for the anodic sludge at the three stages, revealing a total of 1866 operational taxonomic units (OUTs) across all samples. The Original sludge contained 1205 OUTs, Operation sludge had 1075 OUTs, and Shutoff sludge had 655 OUTs. Among these, 223 OUTs were common to all three stages, indicating alterations in microbial community structure with the initiation of system operation. The replacement of azo dye as the catholyte post system initiation created a new environment for microorganisms, instigating changes in the community structure.

The relative abundance plot was constructed based on species annotation results, featuring the top 10 species with the highest abundance at the phylum level in a cumulative bar chart. Fig. 9(a) depicted the relative abundance of microbial community structures at the phylum level for original sludge sediment, sludge during the startup phase, and sludge after the system's operation concludes. Previous studies[44,45] had indicated *Actinobacteria* as the predominant microorganisms in riverbed sediment. As seen in Fig. 9(a), *Actinobacteria* dominate the original sludge sediment, constituting 54.99% of the total microbial population. However, as the microbial system initiates, the abundance of *Actinobacteria* gradually decreased, nearly disappearing when power generation stabilized until the system concludes. Conversely, the abundance of *Proteobacteria* and *Firmicutes*, recognized as major electricity-generating microorganisms[46], increased. Upon stabilization of power generation, *Proteobacteria* exhibited the highest detected quantity, followed by *Bacteroidetes* and *Firmicutes*, constituting 48.54%, 21.56%, and 4.47% of the total detected quantity, respectively.

At the class level, the relative abundance bar chart for the top 10 OUTs was shown in Fig. 9(b). The figure highlighted that after system initiation, *Deltaproteobacteria*, *Alphaproteobacteria*, and *Gammaproteobacteria* from the phylum *Proteobacteria*, along with *Bacteroidia*, *Clostridia*, and *Mollicutes* from the phylum *Firmicutes*, exhibited higher relative abundance in the samples. These classes were known to be electricity-generating bacteria[44]. Following system startup, *Gammaproteobacteria*, as the most significant electricity-generating bacteria, experienced a reduction in relative abundance from the initial 18.32%–8.59% during environmental adaptation, only to increase to 39.71% after full adaptation. When power generation stabilizes, the quantity of known electricity-generating ordered in the anodic membrane increases from 33.41% in the original sludge to 71.24%, contributing to the system's improved electricity-generating performance by providing an ample supply of electrons for the Bio-electro-Fenton process.

Heatmap analysis involved annotating and quantifying species at the genus level for all microbial samples, using a maximum value sorting method. The top 35 genera were selected based on their abundance in each sample, and a heatmap was generated to visually observe differences in microbial composition among samples. Fig. 9(c) illustrated the genus-level clustering of microbial species in the anodic biofilm taken from the system's original sediment sludge, during startup, and after stable system operation. The horizontal axis represented sample codes, while the vertical axis displayed genus annotation information, including the top 35 OUTs at the genus level in terms of relative abundance. The figure highlighted substantial differences in detected microbial species among the three stages. With the initiation of the system, certain initially dominant genera gradually disappeared, and after stable operation, the most predominant genus, *Geobacter*, emerged. *Geobacter* is a typical exoelectrogenic bacterium [47], capable of directly producing extracellular electrons through the oxidation of organic compounds at the anodic electrode. Additionally, it acted as a reductive bacterium for insoluble iron oxides, contributing to the reduction of Fe^{3+} [48]. *Geobacter* can also oxidize aromatic compounds, indicating its potential for the remediation of riverbed sediment.

Another advantageous electrogenic bacterium was *Shewanella*, which thoroughly oxidizes organic acids in the environment.

Complementing the information in class level, *Clostridia*, which utilized sugars and proteins as carbon sources to produce organic acids, were supplemented by *Shewanella*, which oxidizes the metabolites of *Clostridia*. The presence of these two bacteria is highly beneficial for the electrogeneration process.

4. Conclusion

The 3D magnetic graphene material, a kind of graphitic nitrogen material, was prepared to enhance the two-electron pathway, which was beneficial to the bio-electron Fenton system. In the preparation process of the cathode materials, Fe^{2+} as a reduction agent of GO, could trigger ammonia water to form graphitic N in graphene sheets, which could enhance the two-electron pathway to produce H_2O_2 . As cathode material of the bio-electron Fenton system, the maximum output voltage and the maximum power density of N-rGO/ Fe_3O_4 was 0.528 V and 178.17 mW/m². Meanwhile, the MO removal rate was up to 68.91% within 25 h, which should be contributed to the higher concentration of Fe^{2+} and H_2O_2 yield of N-rGO/ Fe_3O_4 . Hence, the 3D magnetic graphene material cathode (N-rGO/ Fe_3O_4) can increase the output voltage and strengthen the catalytic activity of bio-electron Fenton system. Upon system initiation, Actinobacteria in the anodic sediment diminishes, making way for an increase in *Proteobacteria*, *Bacteroidetes*, and *Firmicutes*. These become dominant, constituting 71.24% of electrogenic bacteria post-stable operation. Their prevalence significantly contributes to organic matter degradation, boosting extracellular electron production. This abundance enhances the bio-electro-Fenton process, particularly aiding Methyl Orange (MO) degradation in the cathodic region. This study demonstrated the effectiveness of the 3D magnetic graphene material cathode in the removal of Methyl Orange (MO). Subsequent research should focus more on the mechanism of MO degradation by the Bio-electro-Fenton system, laying the foundation for future practical applications. The application of Sediment Microbial Fuel Cells (SMFCs) in conjunction with synthesized magnetic graphene materials presents a novel approach for not only efficient Methyl Orange (MO) degradation, but also harness energy from microbial activity. This has direct implications for the remediation of water bodies contaminated with organic pollutants, contributing to environmental sustainability.

CRedit authorship contribution statement

Minmin Sun: Writing – original draft, Data curation. **Xiaoli Chai:** Revisions of the manuscript. **Chengxian Wang:** Supervision, Conceptualization.

Declaration of competing interest

The authors declare that they have no known competing financial interests or personal relationships that could have appeared to influence the work reported in this paper.

Acknowledge

This study was financially supported by Ministry of Science and Technology, China [Grant number: 2020YFC1908603] and Interdisciplinary Joint Research and Development Project in 2022, Tongji University, China [Grant number: 2022-4-ZD-01], National Natural Science Foundation of China [Grant number: 52270163]. We are also thankful to the anonymous reviewers for their valuable comments to improve this manuscript.

Appendix A. Supplementary data

Supplementary data to this article can be found online at <https://doi.org/10.1016/j.heliyon.2024.e24772>.

References

- [1] P. Liang, W.L. Wu, J.C. Wei, L.L. Yuan, X. Xia, X. Huang, Alternate charging and discharging of capacitor to enhance the electron production of bioelectrochemical systems, *Environ. Sci. Technol.* 45 (2011) 6647–6653.
- [2] F. Yu, C.X. Wang, J. Ma, Applications of graphene-modified electrodes in microbial fuel cells, *Materials (Basel)* 9 (2016) 27.
- [3] F. Yu, C. Wang, J. Ma, Capacitance-enhanced 3D graphene anode for microbial fuel cell with long-time electricity generation stability, *Electrochim. Acta* 259 (2018) 1059–1067.
- [4] M. Helder, D.P.B.T.B. Strik, H.V.M. Hamelers, C.J.N. Buisman, The flat-plate plant-microbial fuel cell: the effect of a new design on internal resistances, *Biotechnol. Biofuels* 5 (2012).
- [5] R. Rossi, W.L. Yang, L. Setti, B.E. Logan, Assessment of a metal-organic framework catalyst in air cathode microbial fuel cells over time with different buffers and solutions, *Bioresour. Technol.* 233 (2017) 399–405.
- [6] Q. Zhao, M. Ji, R.Y. Li, Z.Y.J. Ren, Long-term performance of sediment microbial fuel cells with multiple anodes, *Bioresour. Technol.* 237 (2017) 178–185.
- [7] C.-X. Wang, F. Yu, J. Ma, Applications of graphene-based hybrid material as electrodes in microbial fuel cells, *Acta Phys. Chim. Sin.* 32 (2016) 2411–2426.
- [8] S. Khilari, S. Pandit, M.M. Ghangrekar, D. Das, D. Pradhan, Graphene supported alpha-MnO₂ nanotubes as a cathode catalyst for improved power generation and wastewater treatment in single-chambered microbial fuel cells, *RSC Adv.* 3 (2013) 7902–7911.
- [9] Q. Zhao, R.Y. Li, M. Ji, Z.J. Ren, Organic content influences sediment microbial fuel cell performance and community structure, *Bioresour. Technol.* 220 (2016) 549–556.

- [10] X. Xu, Q.L. Zhao, M.S. Wu, J. Ding, W.X. Zhang, Biodegradation of organic matter and anodic microbial communities analysis in sediment microbial fuel cells with/without Fe(III) oxide addition, *Bioresour. Technol.* 225 (2017) 402–408.
- [11] Y.N. Zhao, X.F. Li, Y.P. Ren, X.H. Wang, Effect of Fe(III) on the performance of sediment microbial fuel cells in treating waste-activated sludge, *RSC Adv.* 6 (2016) 47974–47980.
- [12] T.-s. Song, Y. Jin, J. Bao, D. Kang, J. Xie, Graphene/biofilm composites for enhancement of hexavalent chromium reduction and electricity production in a biocathode microbial fuel cell, *J. Hazard Mater.* 317 (2016) 73–80.
- [13] Y.B. Fu, Z.H. Liu, G. Su, X.R. Zai, M. Ying, J. Yu, Modified carbon anode by MWCNTs/PANI used in marine sediment microbial fuel cell and its electrochemical performance, *Fuel Cell.* 16 (2016) 377–383.
- [14] D.W. Zhu, D.B. Wang, T.S. Song, T. Guo, P.K. Ouyang, P. Wei, J.J. Xie, Effect of carbon nanotube modified cathode by electrophoretic deposition method on the performance of sediment microbial fuel cells, *Biotechnol. Lett.* 37 (2015) 101–107.
- [15] C.-H. Feng, F.-B. Li, H.-J. Mai, X.-Z. Li, Bio-electro-fenton process driven by microbial fuel cell for wastewater treatment, *Environ. Sci. Technol.* 44 (2010) 1875–1880.
- [16] J. Miao, Y. Fu, B. Peng, Z. Shen, X. Zhou, Y. Zhang, Treatment of sulfonamide antibiotics wastewater by iron-carbon micro- electrolysis process, *China Water & Wastewater* 32 (2016) 96–100.
- [17] W.W. Li, H.Q. Yu, Stimulating sediment bioremediation with benthic microbial fuel cells, *Biotechnol. Adv.* 33 (2015) 1–12.
- [18] X. Li, X. Jin, N. Zhao, I. Angelidakis, Y. Zhang, Novel bio-electro-Fenton technology for azo dye wastewater treatment using microbial reverse-electrodialysis electrolysis cell, *Bioresour. Technol.* 228 (2017) 322–329.
- [19] H. Lin, Y. Lin, L. Liu, Treatment of dinitroazophenol production wastewater by Fe/C and Fe/Cu internal electrolysis and the COD removal kinetics, *J. Taiwan Inst. Chem. Eng.* 58 (2016) 148–154.
- [20] X. Li, B. Hu, S. Suib, Y. Lei, B. Li, Electricity generation in continuous flow microbial fuel cells (MFCs) with manganese dioxide (MnO₂) cathodes, *Biochem. Eng. J.* 54 (2011) 10–15.
- [21] A.-L. Morel, S.I. Nikitenko, K. Gionnet, A. Wattiaux, J. Lai-Kee-Him, C. Labrugere, B. Chevalier, G. Deleris, C. Petibois, A. Brisson, M. Simonoff, Sonochemical approach to the synthesis of Fe₃O₄@SiO₂ core-shell nanoparticles with tunable properties, *ACS Nano* 2 (2008) 847–856.
- [22] J. An, Q. Zhou, M. Wu, L. Wang, Y. Zhong, J. Feng, Y. Shang, Y. Chen, Interactions between oxidative stress, autophagy and apoptosis in A549 cells treated with aged black carbon, *Toxicol. Vitro* 54 (2019) 67–74.
- [23] Q. Yu, X. Jin, Y. Zhang, Sequential pretreatment for cell disintegration of municipal sludge in a neutral Bio-electro-Fenton system, *Water Res.* 135 (2018) 44–56.
- [24] P. Kumari, N. Bahadur, M. Cretin, L. Kong, L.A. O'Dell, A. Merenda, L.F. Dumée, Electro-catalytic membrane reactors for the degradation of organic pollutants – a review, *React. Chem. Eng.* 6 (2021) 1508–1526.
- [25] M. Manna, S. Sen, Advanced oxidation process: a sustainable technology for treating refractory organic compounds present in industrial wastewater, *Environ. Sci. Pollut. Control Res.* 30 (2023) 25477–25505.
- [26] F. Soltani, N. Navidjoui, M. Rahimnejad, A review on bio-electro-Fenton systems as environmentally friendly methods for degradation of environmental organic pollutants in wastewater, *RSC Adv.* 12 (2022) 5184–5213.
- [27] F. Soltani, N. Navidjoui, H. Khorsandi, M. Rahimnejad, S. Alizadeh, A novel bio-electro-Fenton system with dual application for the catalytic degradation of tetracycline antibiotic in wastewater and bioelectricity generation, *RSC Adv.* 11 (2021) 27160–27173.
- [28] Y. Wang, H. Zhang, Y. Feng, B. Li, M. Yu, X. Xu, L. Cai, Bio-Electron-Fenton (BEF) process driven by sediment microbial fuel cells (SMFCs) for antibiotics desorption and degradation, *Biosens. Bioelectron.* 136 (2019) 8–15.
- [29] E. Breslmayr, M. Hanzek, A. Hanrahan, C. Leitner, R. Kittl, B. Šantek, C. Oostenbrink, R. Ludwig, A fast and sensitive activity assay for lytic polysaccharide monoxygenase, *Biotechnol. Biofuels* 11 (2018) 79.
- [30] A.A. Shalaby, A.A. Mohamed, Determination of acid dissociation constants of alizarin red S, methyl orange, bromothymol blue and bromophenol blue using a digital camera, *RSC Adv.* 10 (2020) 11311–11316.
- [31] W.B. Fortune, M.G. Mellon, Determination of iron with o-phenanthroline: a spectrophotometric study, *Ind. Eng. Chem. Anal. Ed.* 10 (1938) 60–64.
- [32] K.S.W. Sing, Reporting physisorption data for gas/solid systems with special reference to the determination of surface area and porosity (Recommendations 1984), *PapCh* 57 (2009) 603–619.
- [33] L.H. Zhou, C.L. Yang, J. Wen, P. Fu, Y.P. Zhang, J. Sun, H.Q. Wang, Y. Yuan, Soft-template assisted synthesis of Fe/N-doped hollow carbon nanospheres as advanced electrocatalysts for the oxygen reduction reaction in microbial fuel cells, *J. Mater. Chem. A* 5 (2017) 19343–19350.
- [34] N. Belachew, D.R. Devi, K. Basavaiah, L-serine-assisted synthesis of Fe₃O₄ impregnated N-doped RGO composites via a facile electrostatic self-assembly for synergistic adsorption of Rhodamine B, *Emergent Mater.* 3 (2020) 63–73.
- [35] J. Geng, Y. Men, C. Liu, X. Ge, C. Yuan, Preparation of rGO@Fe₃O₄ nanocomposite and its application to enhance the thermal conductivity of epoxy resin, *RSC Adv.* 11 (2021) 16592–16599.
- [36] R.P. Zheng, S.J. Liao, S.Y. Hou, X.C. Qiao, G.H. Wang, L.N. Liu, T. Shu, L. Du, A hollow spherical doped carbon catalyst derived from zeolitic imidazolate framework nanocrystals impregnated/covered with iron phthalocyanines, *J. Mater. Chem. A* 4 (2016) 7859–7868.
- [37] M. Descostes, F. Mercier, N. Thromat, C. Beaucaire, M. Gautier-Soyer, Use of XPS in the determination of chemical environment and oxidation state of iron and sulfur samples: constitution of a data basis in binding energies for Fe and S reference compounds and applications to the evidence of surface species of an oxidized pyrite in a carbonate medium, *Appl. Surf. Sci.* 164 (2000).
- [38] Xiaowei Teng, Donald Black, Neil J. Watkins, Yongli Gao, H. Yang, Platinum-maghemite core-shell nanoparticles using a sequential, *Nano Lett.* 3 (2003).
- [39] Y. Pang, H. Xie, Y. Sun, M.-M. Titirici, G.-L. Chai, Electrochemical oxygen reduction for H₂O₂ production: catalysts, pH effects and mechanisms, *J. Mater. Chem. A* 8 (2020) 24996–25016.
- [40] P.-J. Lin, C.-H. Yeh, J.-C. Jiang, Theoretical insight into hydroxyl production via H₂O₂ decomposition over the Fe₃O₄(311) surface, *RSC Adv.* 11 (2021) 36257–36264.
- [41] Z. Deng, X. Wang, Mechanism investigation of enhanced electrochemical H₂O₂ production performance on oxygen-rich hollow porous carbon spheres, *Nano Res.* 15 (2022) 4599–4605.
- [42] V.A. Gomez-Obando, A.M. Garcia-Mora, J.S. Basante, A. Hidalgo, L.A. Galeano, CWPO degradation of methyl orange at circumneutral pH: multi-response statistical optimization, main intermediates and by-products, *Front. Chem.* 7 (2019) 772.
- [43] A.R. Zeradjanin, J. Masa, I. Spanos, R. Schlögl, Activity and stability of oxides during oxygen evolution reaction—from mechanistic controversies toward relevant electrocatalytic descriptors, *Front. Energy Res.* 8 (2021).
- [44] R. Moscoviz, E. Trably, N. Bernet, H. Carrère, The environmental biorefinery: state-of-the-art on the production of hydrogen and value-added biomolecules in mixed-culture fermentation, *Green Chem.* 20 (2018) 3159–3179.
- [45] N. Ryckelynck, H.A. Stecher, C.E. Reimers, Understanding the anodic mechanism of a seafloor fuel cell: interactions between geochemistry and microbial activity, *Biogeochemistry* 76 (2005) 113–139.
- [46] Y.-L. Zhou, H.-L. Jiang, H.-Y. Cai, To prevent the occurrence of black water agglomerate through delaying decomposition of cyanobacterial bloom biomass by sediment microbial fuel cell, *J. Hazard Mater.* 287 (2015) 7–15.
- [47] G. Zhen, X. Lu, G. Kumar, P. Bakonyi, K. Xu, Y. Zhao, Microbial electrolysis cell platform for simultaneous waste biorefinery and clean electrofuels generation: current situation, challenges and future perspectives, *Prog. Energy Combust. Sci.* 63 (2017) 119–145.
- [48] L. De Schampelaire, A. Cabezas, M. Marzorati, M.W. Friedrich, N. Boon, W. Verstraete, Microbial community analysis of anodes from sediment microbial fuel cells powered by rhizodeposits of living rice plants, *Appl. Environ. Microbiol.* 76 (2010) 2002–2008.